




Negative imaginary potential to model ionization in atoms and molecules by electron impactAlan G. Falkowski ¹, Márcio H. F. Bettega ^{2,*} and Marco A. P. Lima ¹¹*Instituto de Física “Gleb Wataghin,” Universidade Estadual de Campinas, 13083-859 Campinas, São Paulo, Brazil*²*Departamento de Física, Universidade Federal do Paraná, Caixa Postal 19044, 81531-980 Curitiba, Paraná, Brazil*

(Received 13 June 2024; accepted 24 July 2024; published 12 August 2024)

The low-energy electron-molecule collisions have several implications for the behavior of microscopic and macroscopic environments. One of the most important consequences of this event is molecular ionization due to the electron impact. Since the inclusion of ionization effects through *ab initio* methods is challenging, we implemented a negative imaginary potential to act as a sinkhole of probability flux to mimic the ionization effects in electron-molecule collisions. We employed an iterative procedure to reproduce the total ionization cross sections computed with the binary-encounter-Bethe model and investigated some Gaussian distributions representing the model potential. Also, in light of obtaining a model with a reasonable physical significance and avoiding arbitrariness, we performed calculations using the probability density as an imaginary potential. Our main goal is to investigate the effect of an absorption potential in the elastic and inelastic channels in *ab initio* calculations using the Schwinger multichannel method. The results obtained in this study using H₂ as a test case are encouraging, since the absorption channel disputes flux probability with other channels.

DOI: [10.1103/PhysRevA.110.022808](https://doi.org/10.1103/PhysRevA.110.022808)**I. INTRODUCTION**

The electron scattering by atoms and molecules has several applications since almost everything in the universe is made from these “small bricks.” In particular, looking into applications, we highlight combustion environments such as atmospheric discharges [1,2], processing plasmas and surface treatments [3–5], nanomaterials manufacturing [6,7], biological medium and chemistry [8–13], biofuels production [14–17], and combustion chambers [18], among others.

Concerning low-energy electron scattering by molecular targets, the Schwinger multichannel (SMC) method [19–22] has proved to be a well-established methodology with successful applications over the years [23–32]. Recently, we applied the SMC method to investigate the electronic excitation of benzene molecules by electron impact and employed 437 open channels in the calculations (elastic plus 436 electronic excitation channels). We observed that the differential cross sections (DCSs) are converged comparing the different levels of calculations. In the results for the elastic channel [33], we obtained an excellent agreement compared to the experimental data available for the electron impact energies (E_0) up to 20 eV. For larger E_0 , for example, 50 eV, the calculations overestimate the experimental data. Regarding electronic excitation [34], our results still overestimate the measured data, even considering a large number of energetically accessible channels derived from the bound Rydberg states below the ionization potential (IP). For intermediate energies (above $E_0 = 20$ eV), the situation is worse, since the results were not improved by increasing the basis set and, as a consequence, the number of channels below the

IP. We suspect that these discrepancies are mostly due to the ionization channels (channels from the continuum, above the first IP threshold) which have not been included in the SMC method up to date.

The SMC method is based on Schwinger’s variational principle, whose kickoff is the Lippmann-Schwinger (LS) equation. However, the LS equation has a limitation in which only one electron in the continuum is allowed (the incident or outgoing electron), since the equation has no unique solution for more electrons in this regime [35]. This makes the *ab initio* approach cumbersome.

In the literature, we cite as examples the following alternative approaches to take ionization effects into account: the R -matrix [36] and convergent close-coupling [37], which uses pseudostates to discretize the continuum of states, and the distorted wave approximation [38], which uses a model imaginary potential to include absorption effects, as electronic excitation plus ionization. In particular, the binary-encounter-Bethe (BEB) model [39] is extremely simple and delivers an equation for the ionization cross section that requires a simple bound-state calculation to obtain orbital constants used as inputs in this approach.

In order to take ionization effects into account in the SMC method, we employed a negative imaginary potential (NIP) in the interaction potential to act as a probability flux sinkhole. We started the initiative to generate a model potential as a single Gaussian function to describe ionization effects by fitting the BEB total ionization cross sections (TICS). However, we observed that the absorption integral cross section (AICS) for this NIP does not have the same magnitude and shape as the BEB TICS. To solve this, the strength of the potential (multiplication constant) is adjusted iteratively for each E_0 to provide an AICS equal to the TICS of the BEB method. In this study, we report the cross sections for elastic and

*Contact author: bettega@fisica.ufpr.br

electronically inelastic scattering of electrons by H_2 . These cross sections were obtained with the SMC method and show the effect of taking ionization into account by including the NIP. Further, we investigate the possibility of giving a physical meaning to the NIP, taking the probability density of the bound electrons as the spatial distribution of the potential.

The remainder of this paper is organized as follows. Section II shows the theory involved in our approach. Section III displays the computational aspects used in the bound-state and scattering calculations. In Sec. IV we display our results and discussions. Section V presents the conclusions and future perspectives.

II. THEORY

A. Prelude

Consider the interaction potential of the form

$$V = V_0 \pm iW_0, \quad (1)$$

where V_0 is the electron-target interact potential and W_0 is an arbitrary potential. As reported in Ref. [35], the presence of $\pm W_0$ in V generates a font (plus sign) or a sinkhole (minus sign) of the current probability density \mathbf{j} (or as usually called, probability flux),

$$\nabla_{\mathbf{r}} \cdot \mathbf{j} = \pm 2W_0 \frac{\partial \rho}{\partial t}, \quad (2)$$

where ρ is the probability density. We are interested in the formalism with $V = V_0 - iW_0$. The behavior of the sinkhole could, in principle, be useful for the absorption of the incident particles. Since an ionized electron (or electrons) goes to the continuum, we could mimic this effect by including a NIP given by Eq. (1) in the scattering dynamics.

B. SMC method with NIP model

After considering the non-Hermitian nature of the Hamiltonian (due to the presence of the NIP) [40], we obtained that the resulting expression of the scattering amplitude is the same as reported elsewhere [19–22] for the real interaction potential. The fixed-nuclei body-frame scattering amplitude is given by

$$f(\mathbf{k}_f, \mathbf{k}_i) = -\frac{1}{2\pi} \sum_{m,n} \langle S_{\mathbf{k}_f} | V | \chi_m \rangle (d^{-1})_{mn} \langle \chi_n | V | S_{\mathbf{k}_i} \rangle, \quad (3)$$

with $d_{mn} = \langle \chi_m | A^{(+)} | \chi_n \rangle$ and

$$A^{(+)} = \frac{\hat{H}}{N+1} - \frac{\hat{H}P + P\hat{H}}{2} + \frac{VP + PV}{2} - VG_p^{(+)}V. \quad (4)$$

In Eq. (4), the reduced Hamiltonian operator $\hat{H} = E - H$ is the total energy (target ground-state energy plus the kinetic energy of the incoming electron) minus the $(N+1)$ -electron Hamiltonian, and N is the number of electrons in the target. The latter is given by $H = H_0 + V$, where H_0 describes the noninteracting electron-molecule system, and $|S_{\mathbf{k}_i}\rangle$ is a solution of H_0 , given by the product of a plane wave with momentum \mathbf{k} and a target state $|\Phi_i\rangle$. The wave vector \mathbf{k}_i (\mathbf{k}_f) is the incoming (outgoing) projectile wave vector. The operator $V = V_0 - iW_0$ is the interaction potential between the incident electron and the molecule V_0 minus i times the potential W_0 . Also, we have the Green's function $G_p^{(+)}$ projected onto

the $P = \sum_{\ell=1}^{N_{\text{open}}} |\Phi_{\ell}\rangle \langle \Phi_{\ell}|$ space, spanning N_{open} electronic target bound states. Our trial $(N+1)$ -electrons scattering wave function is expanded as a combination of states $|\chi_m\rangle$, which are the configuration state functions (CSFs). The practical aspects concerning the CSFs $|\chi_m\rangle$ and the projection operator P are provided in Sec. III.

C. The choices for W_0

We explored two different spatial distributions of W_0 , where both strategies are constructed from a spatial function $V(\mathbf{r})$ multiplied by a function of the electron impact energy E_0 ,

$$W_0 = \zeta_n(E_0)V(\mathbf{r}), \quad (5)$$

with ζ_n being the strength of the potential. We discuss the factor ζ_n later in this section. Motivated by our previous study about a model potential [41], as a first approach, the spatial form chosen for $V(\mathbf{r})$ is an s -type Cartesian Gaussian centered at the origin,

$$V(\mathbf{r}) = C_X e^{-\alpha_X(\mathbf{r})^2}, \quad (6)$$

where C_X is the coefficient and α_X is the exponent of the Gaussian.

As we did not know the correct physical structure of the complex potential, we developed a second approach using the knowledge that the electrons were ionized from the region of the probability density $\rho(\mathbf{r})$, i.e., we settled $V(\mathbf{r}) = \rho(\mathbf{r})$. For a set of atomic orbitals $\{\phi_i; i = 1, \dots, N_{\text{ao}}\}$ inside of the Hartree-Fock (HF) electronic ground state Φ_1 , we have

$$\rho(\mathbf{r}) = \sum_{i=1}^{N_{\text{occ}}} \sum_{j=1}^{N_{\text{ao}}} \sum_{k=1}^{N_{\text{ao}}} C_j^i C_k^i \phi_j(\mathbf{r}) \phi_k(\mathbf{r}) \quad (7)$$

and $C_i^k (C_j^k)$ are the molecular orbital coefficients of the N_{occ} occupied orbitals inside of Φ_1 . For the hydrogen molecule, we have

$$\rho(\mathbf{r}) = \sum_{j=1}^{N_{\text{ao}}} \sum_{k=1}^{N_{\text{ao}}} C_j^1 C_k^1 \phi_j(\mathbf{r}) \phi_k(\mathbf{r}), \quad (8)$$

since we have just one occupied orbital in the electronic ground state. To use $\rho(\mathbf{r})$ as the spatial part of W_0 , it was necessary to implement the matrix elements between the CSFs and the W_0 , which are

$$\langle \chi_m | W_0 | \chi_n \rangle, \quad \langle \chi_m | W_0 P | \chi_n \rangle, \quad \langle \chi_m | P W_0 | \chi_n \rangle. \quad (9)$$

Also, due to the presence of the numerators of Eq. (3) and the Green's operator matrix elements, we had to implement in the SMC method code the matrix elements given by $\langle \chi_m | W_0 | \Phi_{\ell} \mathbf{k} \rangle$. As W_0 is a one-electron operator, the primitive integrals involving the probability density are the four-center overlap integrals

$$\int d^3r (x - A_x)^{n_{ax}} (y - A_y)^{n_{ay}} (z - A_z)^{n_{az}} e^{-\alpha_A(\mathbf{r}-\mathbf{A})^2} \times \rho(\mathbf{r}) (x - B_x)^{n_{bx}} (y - B_y)^{n_{by}} (z - B_z)^{n_{bz}} e^{-\alpha_B(\mathbf{r}-\mathbf{B})^2} \quad (10)$$

and the Fourier transform of three-center overlap integrals

$$\int d^3r (x - A_x)^{n_{ax}} (y - A_y)^{n_{ay}} (z - A_z)^{n_{az}} e^{-\alpha_A(\mathbf{r}-\mathbf{A})^2} \rho(\mathbf{r}) e^{+i\mathbf{k}\cdot\mathbf{r}}, \quad (11)$$

where \mathbf{A} and \mathbf{B} are arbitrary Cartesian vectors, and α_A and α_B are arbitrary Gaussian exponents. This second representation of W_0 helps us to obtain a spatial distribution for the NIP instead of using a single Gaussian with an arbitrary width.

D. Cross sections and the iterative factor ζ_n

The integral cross section (ICS) is given by

$$\sigma_{i \rightarrow f} = \frac{1}{4\pi} \frac{k_f}{k_i} \int d\hat{k}_i \int d\hat{k}_f |f(\mathbf{k}_f, \mathbf{k}_i)|^2, \quad (12)$$

where the integral $\frac{1}{4\pi} \int d\hat{k}_i$ is to ensure the average over all target orientations. From Eq. (12), setting $|\mathbf{k}_i| = |\mathbf{k}_f|$ we obtain the elastic ICS (ECS), σ_{ecs} . The inelastic cross sections (INECS) were obtained by summing all cross sections from transitions for an initial state i to a final state f :

$$\sigma_{\text{inecs}} = \sum_{f=2}^{N_{\text{open}}} \sigma_{i \rightarrow f}, \quad (13)$$

where for $i = f = 1$ we have the ECS. Therefore, the total ICS (TCS) could be obtained from the optical theorem (OPTH) as

$$\sigma_{\text{opt}} = \frac{1}{4\pi} \int d\hat{k}_i \frac{4\pi}{k_i} \text{Im} [f(\mathbf{k}_i, \mathbf{k}_i)]. \quad (14)$$

Due to the presence of the NIP, $\sigma_{\text{opt}} - \sigma_{\text{ecs}} \neq \sigma_{\text{inecs}}$, since now we have the absorption of the incident flux, i.e., an absorption ICS (the AICS). Therefore,

$$\sigma_{\text{opt}} - \sigma_{\text{ecs}} - \sigma_{\text{inecs}} \equiv \sigma_{\text{aics}}. \quad (15)$$

Now we can rescue the discussion of the factor ζ_n , named the iteration factor. In our iterative procedure, the objective is to adjust the factor ζ_n until $\sigma_{\text{aics}, n-1}$ is equal to σ_{BEB}

$$\zeta_n = \frac{\sigma_{\text{BEB}}}{\sigma_{\text{aics}, n-1}} \beta_1 + \zeta_{n-1} \beta_0, \quad (16)$$

where n is the iteration number, with ζ_0 being an arbitrary number, usually 1 hartree. We have chosen $\beta_1 = 0.1$ and $\beta_0 = 0.9$, i.e., 10% to increment ζ_{n-1} by the ratio of σ_{BEB} by $\sigma_{\text{aics}, n-1}$ and 90% from the previous iteration. The σ_{BEB} is the BEB model partial ionization cross section given by

$$\sigma_{\text{BEB}} = \frac{S}{t+u+1} \left[\frac{\ln t}{2} \left(1 - \frac{1}{t^2} \right) + 1 - \frac{1}{t} - \frac{\ln t}{t+1} \right], \quad (17)$$

where $S = 4\pi a_0^2 N(R/B)^2$ ($R = 13.6057$ eV), B is the orbital binding energy, U is the orbital kinetic energy ($u = U/B$), and T is the incident energy ($t = T/B$). To obtain the TICS, one should sum the contribution of each occupied orbital. Note that the BEB model is just a parameter for the NIP, meaning that we could use any other ionization cross sections, including experimental ones. In summary, we perform the SMC method scattering calculations, obtain $\sigma_{\text{aics}, n-1}$, and verify the convergence of the factor ζ_n , which is achieved

TABLE I. Exponents of the uncontracted Cartesian Gaussian functions of s , p , and d types, for target and scattering calculations. Please see the text for more details.

Target and scattering description		Extra functions for scattering
s	p	d
39.186 359	1.475 474 7	4.5
6.567 806 2	0.339 955 51	1.5
1.774 537 5	0.109 565 38	0.5
0.623 416 84	0.042 477 76	0.125
0.235 659 27	0.017 663 03	0.031 25
0.089 189 09	0.006 933 56	
0.036 337 81		
0.015 303 56		
0.005 615 93		

when $\sigma_{\text{aics}, n-1} = \sigma_{\text{BEB}}$. If the iterative procedure does not converge, we update the iterative factor and perform the scattering calculations again. This procedure is repeated until ζ_n is converged. The uncertainty assumed for the convergence is about $|\sigma_{\text{aics}, n-1} - \sigma_{\text{BEB}}|^2 \approx 0.1\%$ of σ_{BEB} .

III. COMPUTATIONAL ASPECTS

The geometry of the H_2 molecule used in all calculations ($R_0 = 1.401 a_0$) was obtained from the experimental data available in the CCCBDB Nist Database [42]. Table I shows the Cartesian Gaussian functions used to represent the atomic orbitals utilized in this study. We employed the s and p basis set as Natalense *et al.* [43] used in their calculations. We supplemented the scattering basis with Δ -type functions as scattering orbitals from the work of da Costa *et al.* [44]. The linear combinations of d orbitals employed to generate only Δ -type orbitals were $(d_{x_1^2} - d_{y_1^2}) \pm (d_{x_2^2} - d_{y_2^2})$ and $d_{x_1 y_1} \pm d_{x_2 y_2}$, where the indexes 1 and 2 correspond for each atom of the hydrogen molecule.

The electronic ground state was obtained in the HF approximation, where the canonical virtual orbitals are improved by using the modified virtual orbitals (MVO) technique [45], as implemented in the GAMESS computational package [46]. The MVO approach employed was to diagonalize the electronic Hamiltonian of the target where the occupied molecular orbital σ_g was half-filled, i.e., for the target H_2^+ .

Going to the computational description of the scattering problem, we performed two multichannel scattering calculations to verify the influence of the NIP. We give here a detailed description of each one.

(i) The 3-channel (3ch) calculation ($N_{\text{open}} = 3$): the elastic channel (ground state $X^1\Sigma_g$) and the electronic excitation channels from the $X^1\Sigma_g$ state to the $b^3\Sigma_u^{(+)}$ and $B^1\Sigma_u^{(+)}$ states. The configuration interaction singles (CIS) description was obtained from a single excited determinant constructed from the highest occupied molecular orbital (HOMO)-lowest unoccupied molecular orbital (LUMO) excitation. The vertical excitation energies for 3ch calculations are shown in Table II, in comparison with calculations and experiments from the literature [47–50].

(ii) The 39-channel (39ch) calculation ($N_{\text{open}} = 39$): includes all the channels in the 3ch calculation and 36 more

TABLE II. Vertical excitation energies (in eV) at the TCIS and CIS levels compared to the FCIS calculation. We compare our results with the R -matrix full configuration interaction (FCI) and molecular convergent close-coupling (MCCC) configuration interaction (CI) calculations from Ref. [50] (both calculations at the bond length $R_0 = 1.448 a_0$) and experimental data from Sharp [47], Wrkich *et al.* [49] and Hargreaves *et al.* [50]. The CIS calculation corresponds to the level of description of excited states in the 3ch calculation (only one hole-particle pair to describe the excited states) and the TCIS with the 39ch calculation (nineteen hole-particle pairs to describe the excited states).

Symmetry	FCIS	CIS	TCIS	R -matrix FCI	MCCC CI	Sharp	Wrkich	Hargreaves
$b^3\Sigma_u$	9.97	10.09	10.04	10.23	10.31			
$a^3\Sigma_g$	12.03		12.05	12.35	12.14		11.79	11.78
$c^3\Pi_u$	12.31		12.32	12.52	12.35	11.76	11.79	11.76
$B^1\Sigma_u$	12.73	13.75	12.97	12.52	12.44	11.18	11.18	11.17
$E(F)^1\Sigma_g$	13.00		13.10	12.93	12.73	12.29	12.30	12.29
$C^1\Pi_u$	13.09		13.17	13.02	12.73	12.29	12.30	12.28

electronic excitation channels. In Table II, we show the vertical excitation energies for the states discussed in Sec. IV. We employed the truncated CIS (TCIS) [28] to select all-important single excitations from the full CIS (FCIS) calculation to describe all the states up to the cutoff energy given by ϵ_P . We chose $\epsilon_P = \text{IP} = 16.17$ eV, which is the IP of the hydrogen molecule according to Koopmans' theorem calculated with the HF orbital energy. This gives rise to 38 excited states (half singlets and half triplets) below the ϵ_P . Table II also shows this comparison for a TCIS using 19 excited determinants (made with 19 hole-particle pairs) and the FCIS calculation.

As mentioned in Sec. II, we need to define the CSFs used in the scattering calculations. The electronic ground state and single excitations from the CIS were employed as target determinants in $|\chi_m\rangle$. The scattering orbitals are all the

virtual orbitals obtained from the MVO approach from the HF target. This strategy enables us to consider all channels open in each calculation mentioned (3ch and 39ch), where the number of CSFs used was different for each calculation level (230 and 2642 CSFs, respectively). This ensures that we avoid pseudoresonances from closed channels. Furthermore, we maintain only CSFs of doublet multiplicity.

For the 3ch calculations, we tested different values of α , corresponding to different widths of the Gaussian function within W_0 . The values chosen were $\alpha = 1, 2, 4, \text{ and } 8 a_0^{-2}$. Additionally, W_0 was constructed linearly proportional to the electronic probability density $[\rho(\mathbf{r})]$. The $\rho(\mathbf{r})$ used was obtained in the HF approximation (ground state) for all the multichannel coupling calculations. Finally, the initial iterative factor was set to $\zeta_0 = 1$ hartree, except for $\rho(\mathbf{r})$ in the 39ch calculation, where we used $\zeta_0 = 0.1$ hartree.

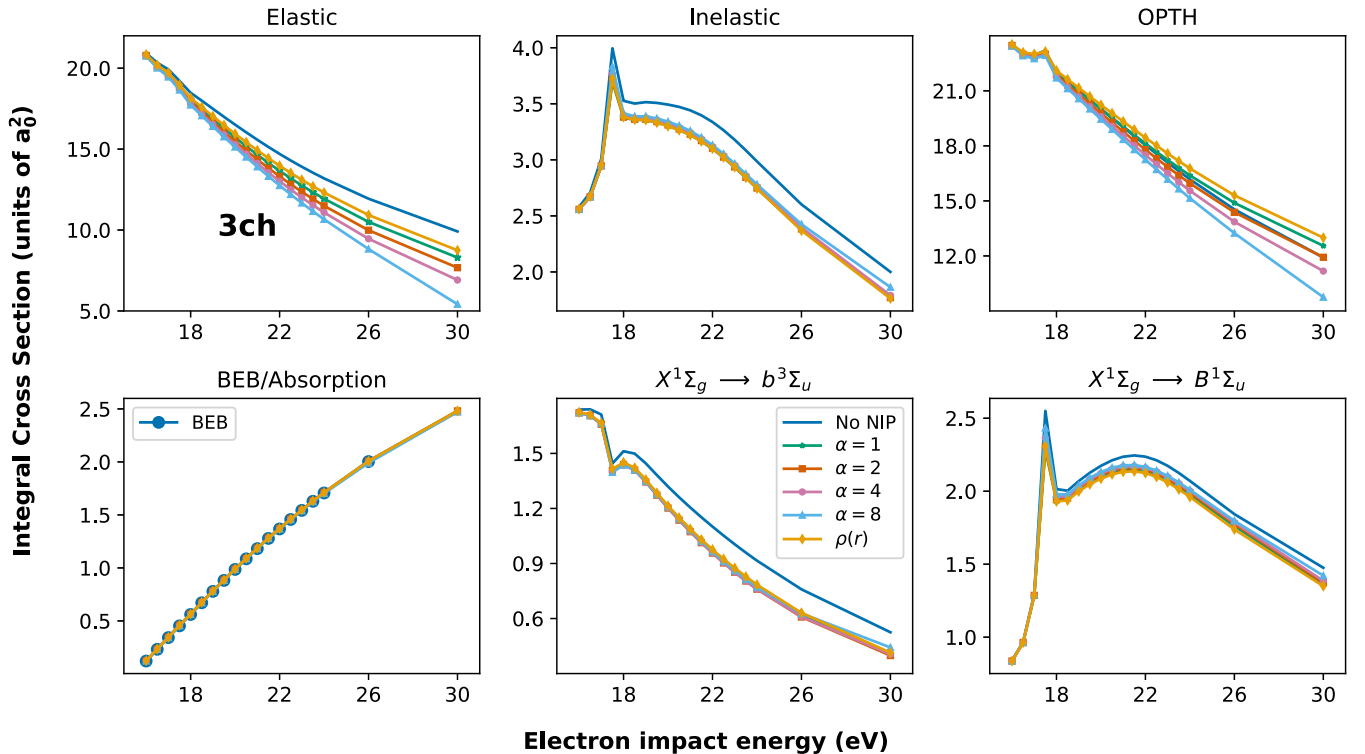


FIG. 1. Elastic, inelastic, total (OPTH), and electronic excitation integral cross sections for electron scattering by H_2 molecules for the cases without and with the NIP model inclusion.

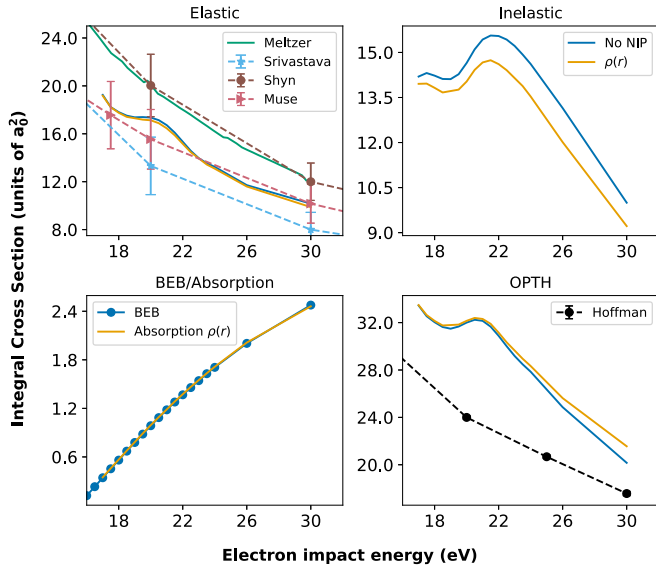


FIG. 2. Elastic, inelastic, absorption, and total (OPTH) integral cross sections for electron scattering by H_2 molecules for the cases without and with the NIP model inclusion, for 39ch. We compare our calculations with the theoretical work (MCCC) of Meltzer *et al.* [48] and the experimental data of Srivastava *et al.* [51], Hoffman *et al.* [54], Shyn and Sharp [52], and Muse *et al.* [53].

IV. RESULTS

A. Integral cross sections for 3ch calculations

Let us highlight the main features generated by the inclusion of the NIP. Figure 1 shows the results from the 3ch calculations. The elastic integral cross section decreases as the electron incident impact energy (E_0) increases, mimicking the flux competition between the elastic and inelastic channels. The results clearly show that the AICS (flux absorbed by the sinkhole) is parametrized iteratively to reproduce the BEB TICS. Looking at the electronic excitation channels, the drop in the cross sections caused by the NIP is different for the singlet and triplet transitions. This means that the NIP also works in the inelastic channels since our model disputes probability flux differently for each state. The TCS (OPTH) is shown by completeness and carries the influence of the NIP as well. Also, the OPTH cross sections show an interesting behavior, since for $\alpha = 1 a_0^{-2}$ and $\rho(\mathbf{r})$ the magnitude of the cross sections increases according to the increase of E_0 . This could be expected by including the ionization effects, which also contribute to the total scattering. For the inelastic channels, the change in the Gaussian width slightly modifies the cross-section magnitudes. This challenged us to explain the correct physical meaning of a given complex potential. Our first attempt was to use the probability density $\rho(\mathbf{r})$ as the spatial part. We verified that the NIP behaves similarly to a Gaussian distribution with diffuse exponents since the elastic cross sections have magnitudes above those of the case with $\alpha = 1 a_0^{-2}$. The advantage of using $\rho(\mathbf{r})$ is to remove the arbitrariness in choosing the Gaussian width within the NIP. Furthermore, the physical meaning of the NIP with $\rho(\mathbf{r})$ as its spatial part is that the flux probability is stolen from the region where the electrons can be localized in the molecule. The

peak appearing in the curves around 17.5 eV is noticeable and was investigated and classified as spurious caused by linear dependence in the basis set. Moreover, the associated CSF is $|\chi_m\rangle = \mathcal{A}|\Phi_{\text{HOMO}}^{\text{LUMO}}\rangle \otimes |\phi_{\text{LUMO}}\rangle$, where, in this case, $|\Phi_{\text{HOMO}}^{\text{LUMO}}\rangle$ is a singlet excited determinant generated from the HOMO-LUMO excitation. We decided to maintain the basis set since the main objective of this work is to evaluate the influence of the NIP in the scattering dynamics.

B. Integral cross sections for 39ch calculations

The expected effects of the inclusion of NIP in the 3ch calculation were detected, but the question is: does the same occur when more energetically accessible channels are included in the calculations? Once we know the effect of the NIP, it is time to include the TCIS strategy to allow more channels to be open, calling the combined strategy TCIS + NIP. Figure 2 shows the results of ECS, INECS, AICS, and TCS (OPTH) obtained with the 39ch calculation, compared with the MCCC calculations of Meltzer *et al.* [48] and experimental data available in the literature [51–55]. We take into account all open channels energetically accessible above the IP and the absorption due to the NIP to mimic the TICS of the BEB model. Also, it is important to recall that we use the probability density to force the flux absorption in the regions most likely occupied by electrons. The agreement between our results and experimental data for the elastic channel is good. Our results underestimate the MCCC calculations in magnitude by approximately 17%, where these very sophisticated calculations are in excellent agreement with the measurements of Ref. [52]. It is worth mentioning that our goal is not to obtain accurate cross sections for the hydrogen molecule; instead of this we want to evaluate the influence of the NIP to mimic the ionization effects. The INECS calculated with NIP underestimates the no NIP calculations, which is expected since the sum of all electronic excitation cross sections is smaller due to the probability of flux absorption. Regarding the TCS, our results overestimate the measurement points. Again, it is noticeable that our TCS with NIP has the correct behavior by increasing the impact energy E_0 , which is the growth in magnitude compared to the no NIP calculation. Figure 3 shows the electronic excitation cross sections obtained with the 39ch calculation, compared again with the MCCC calculations of Meltzer *et al.* [48] and measurements available in the literature [49,50,55,56]. The results reinforce the ideas discussed above for the 3ch calculation. In addition, the effect of the NIP in each electronic excitation channel shows that the flux probability sinkhole acts differently for each transition. Considering the excitation to the first triplet excited state ($X^1\Sigma_g \rightarrow b^3\Sigma_u$), the cross sections are very close to the experiment, where the inclusion of the NIP improves the comparison. For the transition to the first singlet excited state ($X^1\Sigma_g \rightarrow B^1\Sigma_u$), the cross sections overestimate the experimental data up to 20 eV, and again, the NIP brings our results towards the experimental points. As the first singlet transition has a transition dipole moment, for larger energies (above 20 eV), we expect that our calculations underestimate the experimental data, since the importance of this effect increases with E_0 . The other electronic excitation channels overestimate the experimental curves. These discrepancies can be attributed to the lack of

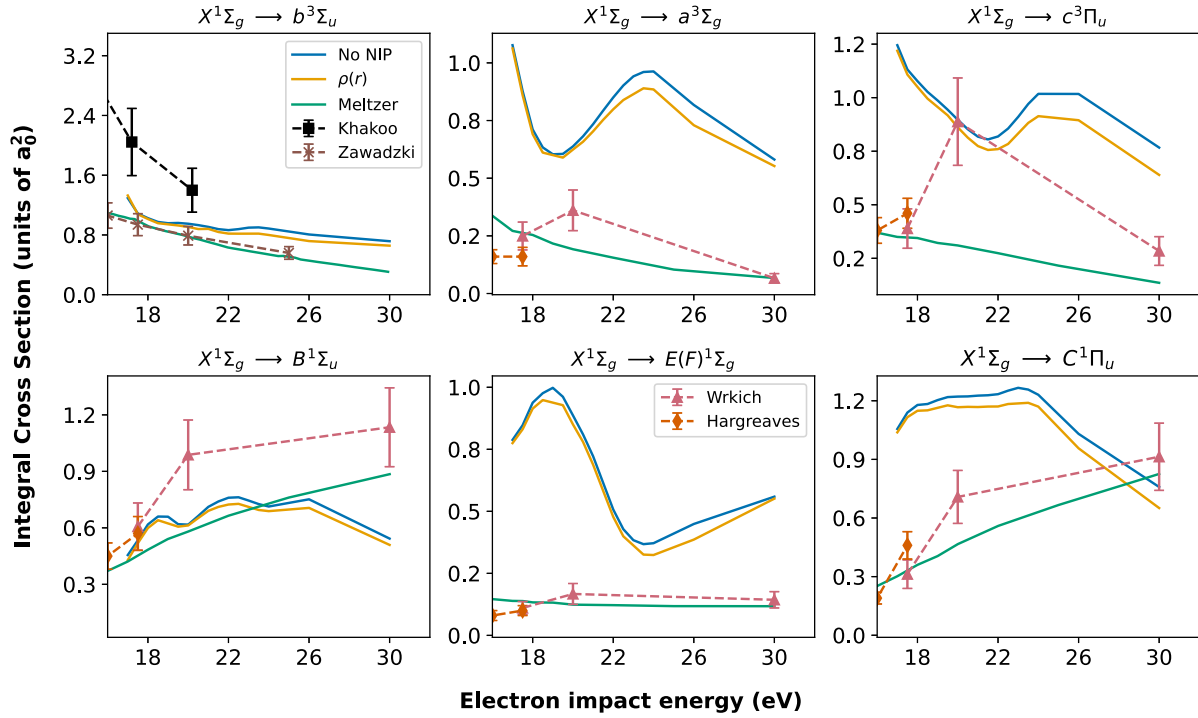


FIG. 3. Electronic excitation integral cross sections for electron scattering by H_2 molecules for the cases without and with the NIP model inclusion, for 39ch. We compare our calculations with the theoretical work (MCCC) of Meltzer *et al.* [48] and the experimental data of Khakoo and Segura [55], Wrkich *et al.* [49], Hargreaves *et al.* [50], and Zawadzki *et al.* [56].

long-range interactions (due to using L^2 functions), which are very important to the dipole-allowed transitions and can unbalance the multichannel coupling.

C. Iterative factor ζ_n

Considering all the different widths of the Gaussian used ($\alpha = 1, 2, 4,$ and $8 a_0^{-2}$) in the 3ch calculations (Fig. 1), we observed a progressive decrease in the magnitude of the elastic

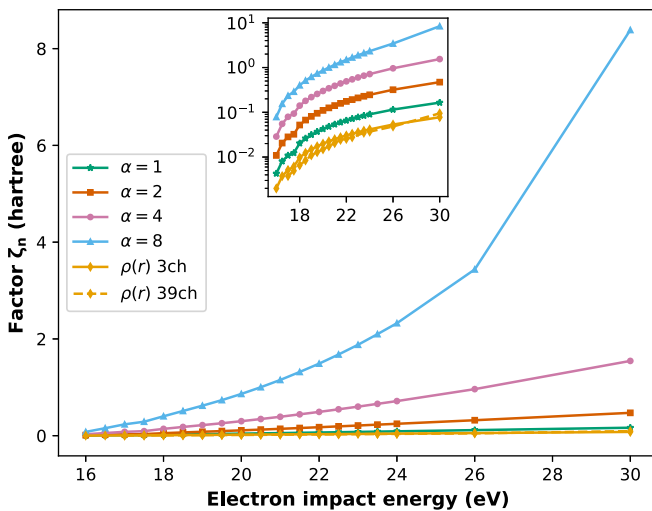


FIG. 4. Factor ζ_n as a function of impact electron energy E_0 for different NIP model spatial distributions. The α values correspond to the 3ch calculations in Fig. 1.

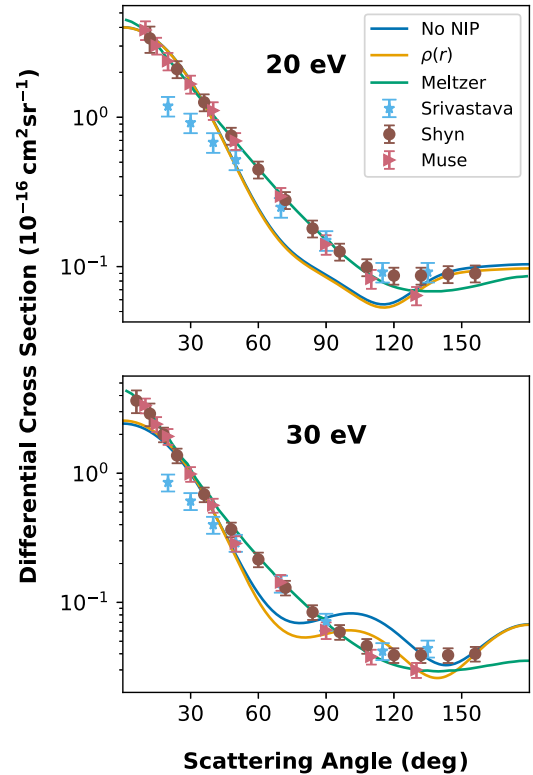


FIG. 5. Elastic differential cross sections for electron scattering by H_2 molecules for the cases without and with the NIP model inclusion, for 39ch. We compare our calculations with the theoretical work (MCCC) of Meltzer *et al.* [48] and the experimental data of Srivastava *et al.* [51], Shyn and Sharp [52], and Muse *et al.* [53].

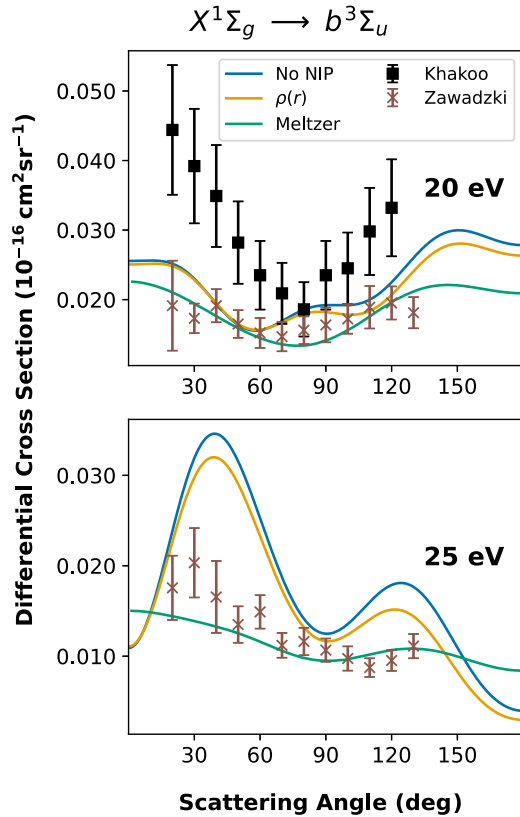


FIG. 6. Differential cross sections for the transition $X^1\Sigma_g \rightarrow b^3\Sigma_u$ of the electron scattering by H_2 molecules for the cases without and with the NIP model inclusion, for 39ch. We compare our calculations with the theoretical work (MCCC) of Meltzer *et al.* [48] and experimental data of Khakoo and Segura [55] and Zawadzki *et al.* [56].

cross section with the increasing value of α . Figure 4 shows different ζ_n values as a function of E_0 and that the magnitude of ζ_n increases with increasing values of α . This indicates that for a given NIP, the adjustment of ζ_n is done to compensate for the spatial part, which needs to steal the probability flow as per the BEB model. The iterative factor involving $\rho(\mathbf{r})$ has small magnitudes compared to those of other spatial distributions, implying that the spatial component of W_0 predominantly gives absorption in the BEB model quality. Furthermore, we notice that the ζ_n values obtained for the 3ch and 39ch calculations using $\rho(\mathbf{r})$ as the spatial part of the NIP are very close in magnitude. This indicates that we can use a small open channel space calculation to obtain the iterative factor and use it as a kickoff for a more sophisticated calculation.

D. Differential cross sections

A more direct comparison between our calculations and the experimental results is possible via the DCSs, avoiding the extrapolation for scattering angles (θ) that the experimentalists cannot access via measurements.

The DCSs for the elastic channel are shown in Fig. 5. In general, our calculations have a reasonable agreement with the experimental data available, where the accord is less appreciable in the intermediate angles range (between 30° and 120°).

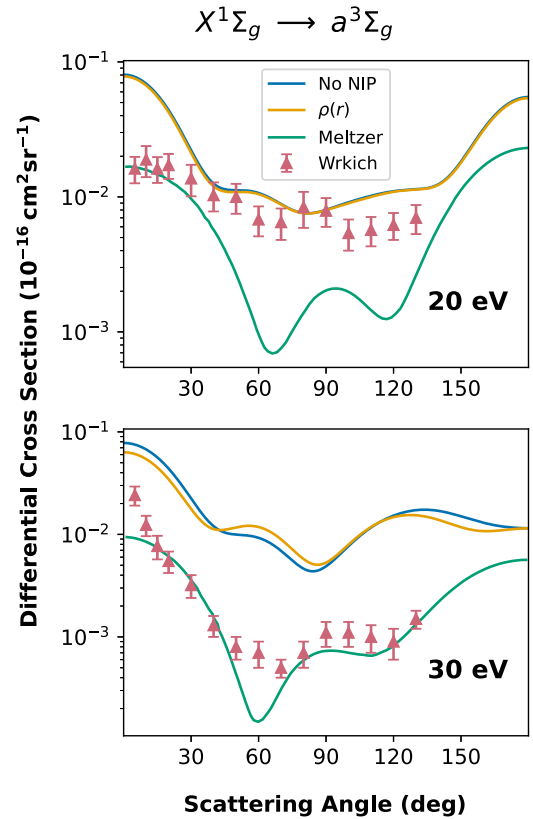


FIG. 7. Differential cross sections for the transition $X^1\Sigma_g \rightarrow a^3\Sigma_g$ of the electron scattering by H_2 molecules for the cases without and with the NIP model inclusion, for 39ch. We compare our calculations with the theoretical work (MCCC) of Meltzer *et al.* [48] and the experimental data of Wrkich *et al.* [49].

The MCCC calculations by Meltzer *et al.* [48] have a good agreement with the measurements for small and intermediate angles, while for large θ the agreement is not as good. The influence of the NIP inclusion is noticeable by looking at the $E_0 = 30$ eV, where the agreement between our calculations and the experimental points is improved. Also, the drop in magnitude caused by the flux absorption is more evident in the DCSs than in the ICSs (Fig. 2). These results also showed that, although the NIP was parametrized through AICSS, it displayed the correct physical behavior in the DCSs.

Regarding the electronic excitation for the triplet excited states, we show the results in Figs. 6–8. Here some controversies appear since for $E_0 = 20$ eV the agreement of our computed DCSs with the experimental data is exceptional while at 30 eV (25 eV for the $X^1\Sigma_g \rightarrow b^3\Sigma_u$ transition), the agreement between the MCCC calculations and the experimental data is better than that with our SMC calculations. These results highlight the importance of more theoretical and experimental efforts to understand the correct nature of electron-molecule scattering. Considering the inclusion of the NIP in our calculations, the results indicate that the flux absorption is different for each electronic excitation transition, which improves the comparison with the measurements.

Concerning the transition for the singlet excited states, the results are shown in Figs. 9–11. For these electronic excitation channels, we also observe the controversies raised in the

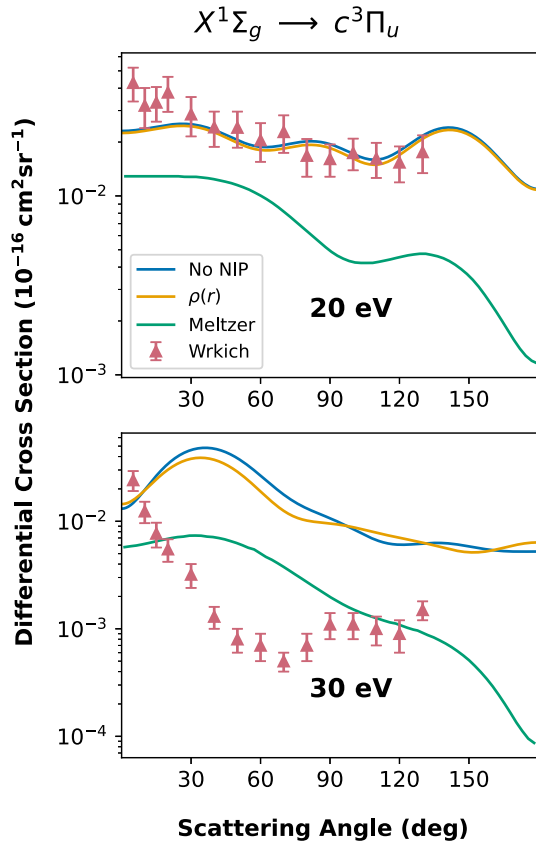


FIG. 8. As in Fig. 6, but for the transition $X^1\Sigma_g \rightarrow c^3\Pi_u$.

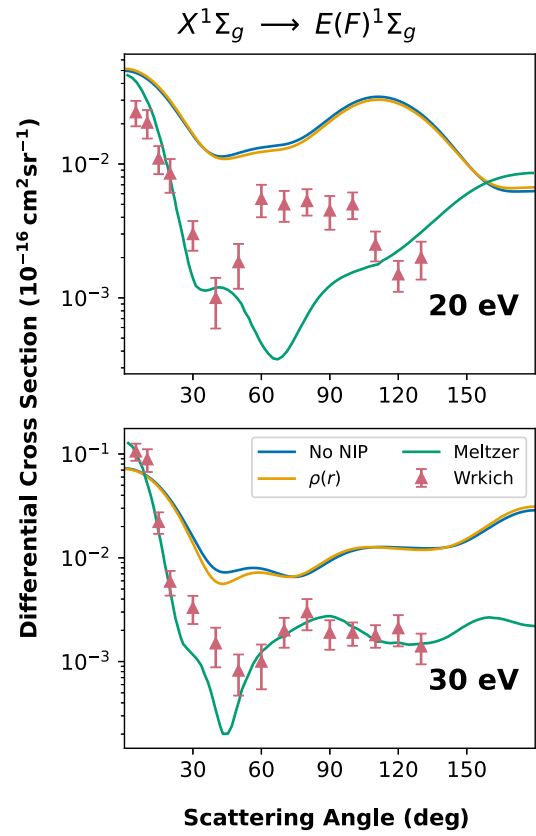


FIG. 10. As in Fig. 6, but for the transition $X^1\Sigma_g \rightarrow E(F)^1\Sigma_g$.

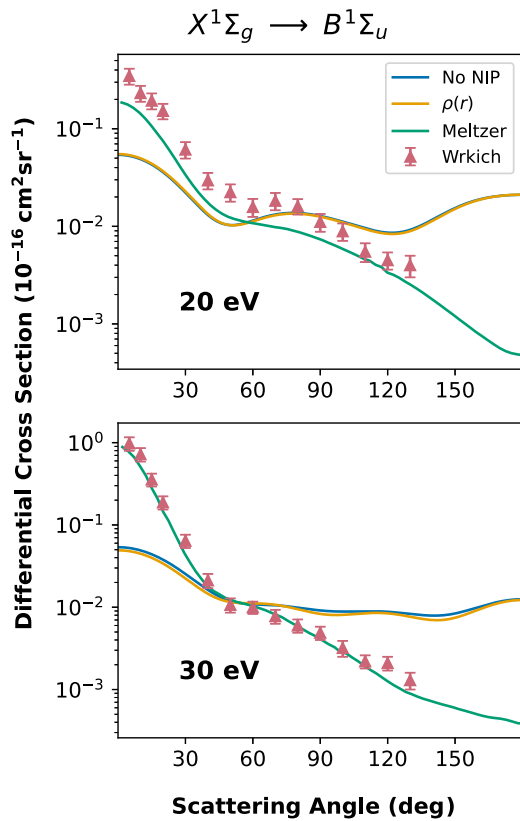


FIG. 9. As in Fig. 6, but for the transition $X^1\Sigma_g \rightarrow B^1\Sigma_u$.

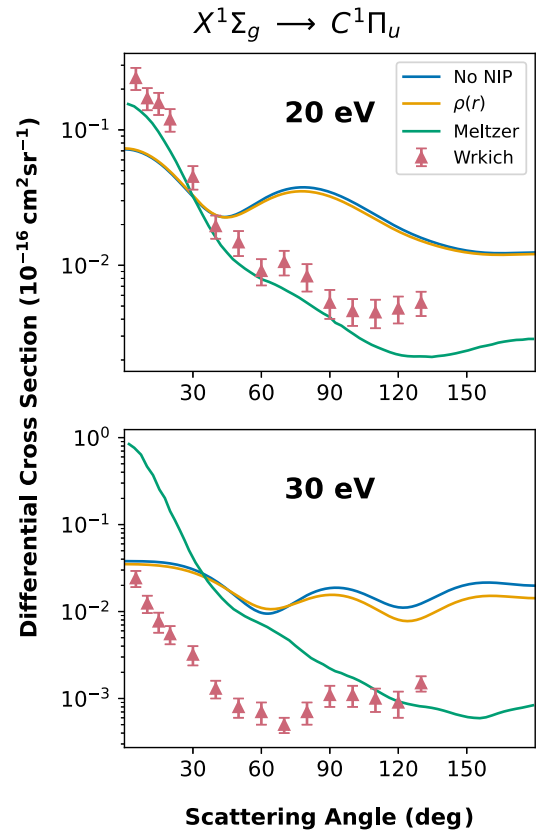


FIG. 11. As in Fig. 6, but for the transition $X^1\Sigma_g \rightarrow C^1\Pi_u$.

previous paragraph. The long-range interactions, such as the interaction between the incident electron electric field and the dipole/transition dipole moment, characteristically influence the scattering at low angles ($<30^\circ$). In this study, we have not used any approach to correct this angular range. As a consequence, the DCSs at small angles are poorly described using the SMC method, while the MCCC calculation provided results in better agreement with the experimental data. The comparison between theory and experiment reinforces the need for more studies of electron scattering by atoms and molecules.

V. CONCLUSIONS

We presented a strategy to include the ionization effects via a negative imaginary potential model called NIP, which was implemented in the Schwinger multichannel method. This general approach can be implemented in other *ab initio* and model potential methods as well. We evaluated the influence of the NIP for the electron scattering by H_2 molecules up to electron impact energies of 30 eV. The results presented in this study show the effectiveness of the NIP in absorbing flux probability as the TICS with BEB model quality. Note that the BEB TICS is just a parameter, which can be replaced for TICSs obtained from other more robust methods [57] and even the experimental data. The expected behavior of stealing probability flux can be seen through the drop in the magnitude of the elastic cross section due to the inclusion of the NIP, compared to calculations without the model. Furthermore, the spatial shape of the NIP does not strongly affect the cross sections of the electronic excitation channels. It is important to notice that the maximum of the TICS for the hydrogen molecule is around 70 eV (with $\sigma_{\text{BEB}} \approx 3.64 a_0^2$); therefore, we expected that the drop in magnitude of the cross sections up to 30 eV (at this energy, $\sigma_{\text{BEB}} \approx 2.48 a_0^2$) by the

inclusion of the NIP model to be moderated. Further studies will be realized for larger molecules, which have the peak of the TICS in lower energies (for example, benzene [58]) to provide a more evident effect of flux probability absorption by the NIP. In addition, we removed the spatial distribution arbitrariness of the Gaussian function by including the probability density as the NIP. Our calculations for the integral cross sections were compared with the MCCC calculations [48] and experimental data available in the literature [49–56]. The agreement is good for the elastic channel and the first triplet excitation; in contrast, for the other channels, the agreement is not as good. We also reported the DCSs for all energetically allowed channels, highlighting the importance of more theoretical investigations in electron-molecule scattering since no one method has the absolute description of the experimental data and more measurements are needed to confirm this idea. We can then say that the role of the NIP in the SMC method is being fulfilled since the expected behavior (and also unexpected positive results) occurs.

ACKNOWLEDGMENTS

A.G.F. acknowledges support from Coordenação de Aperfeiçoamento de Pessoal de Nível Superior, Brasil (CAPES), Finance Code 001. This research used the computing resources and assistance of the John David Rogers Computing Center (CCJDR) in the Institute of Physics “Gleb Wataghin,” University of Campinas. This work also used resources of the “Centro Nacional de Processamento de Alto Desempenho em São Paulo (CENAPAD-SP).” M.H.F.B. acknowledges support from the Brazilian agencies Conselho Nacional de Desenvolvimento Científico e Tecnológico (CNPq) and computational support from Prof. Carlos M. de Carvalho at LFTC-DFis-UFPR and at LCPAD-UFPR.

-
- [1] P. V. Johnson, C. P. Malone, M. A. Khakoo, J. W. McConkey, and I. Kanik, *J. Phys.: Conf. Ser.* **88**, 012069 (2007).
- [2] L. Campbell and M. J. Brunger, *Plasma Sources Sci. Technol.* **22**, 013002 (2012).
- [3] W. M. Huo and Y. K. Kim, *IEEE Trans. Plasma Sci.* **27**, 1225 (1999).
- [4] C. Winstead and V. McKoy, in *Advances in Atomic, Molecular, and Optical Physics*, edited by B. Bederson and H. Walther (Elsevier, Amsterdam, 2000), Vol. 43, pp. 111–145.
- [5] L. G. Christophorou and J. K. Olthoff, *Appl. Surf. Sci.* **192**, 309 (2002).
- [6] W. F. van Dorp, *Phys. Chem. Chem. Phys.* **14**, 16753 (2012).
- [7] W. F. van Dorp, X. Zhang, B. L. Feringa, T. W. Hansen, J. B. Wagner, and J. T. M. De Hosson, *ACS Nano* **6**, 10076 (2012).
- [8] B. Boudaiffa, P. Cloutier, D. Hunting, M. A. Huels, and L. Sanche, *Science* **287**, 1658 (2000).
- [9] M. A. Huels, I. Hahndorf, E. Illenberger, and L. Sanche, *J. Chem. Phys.* **108**, 1309 (1998).
- [10] X. Pan, P. Cloutier, D. Hunting, and L. Sanche, *Phys. Rev. Lett.* **90**, 208102 (2003).
- [11] L. Sanche, *Eur. Phys. J. D* **35**, 367 (2005).
- [12] E. Alizadeh and L. Sanche, *Chem. Rev.* **112**, 5578 (2012).
- [13] J. D. Gorfinkiel and S. Ptasińska, *J. Phys. B: At. Mol. Opt. Phys.* **50**, 182001 (2017).
- [14] A. J. Ragauskas, C. K. Williams, B. H. Davison, G. Britovsek, J. Cairney, C. A. Eckert, W. J. Frederick, J. P. Hallett, D. J. Leak, C. L. Liotta, J. R. Mielenz, R. Murphy, R. Templer, and T. Tschaplinski, *Science* **311**, 484 (2006).
- [15] J. Amorim, C. Oliveira, J. A. Souza-Corrêa, and M. A. Ridenti, *Plasma Processes Polym.* **10**, 670 (2013).
- [16] M. A. Ridenti, J. A. Filho, M. J. Brunger, R. F. da Costa, M. T. do N. Varella, M. H. F. Bettega, and M. A. P. Lima, *Eur. Phys. J. D* **70**, 161 (2016).
- [17] M. J. Brunger, *Int. Rev. Phys. Chem.* **36**, 333 (2017).
- [18] C. D. Cathey, T. Tang, T. Shiraiishi, T. Urushihara, A. Kuthi, and M. A. Gundersen, *IEEE Trans. Plasma Sci.* **35**, 1664 (2007).
- [19] K. Takatsuka and V. McKoy, *Phys. Rev. A* **24**, 2473 (1981).
- [20] K. Takatsuka and V. McKoy, *Phys. Rev. A* **30**, 1734 (1984).
- [21] M. A. P. Lima, L. M. Brescansin, A. J. R. da Silva, C. Winstead, and V. McKoy, *Phys. Rev. A* **41**, 327 (1990).
- [22] R. F. da Costa, M. T. do N. Varella, M. H. F. Bettega, and M. A. P. Lima, *Eur. Phys. J. D* **69**, 159 (2015).

- [23] R. F. da Costa, M. H. F. Bettega, M. A. P. Lima, M. C. A. Lopes, L. R. Hargreaves, G. Serna, and M. A. Khakoo, *Phys. Rev. A* **85**, 062706 (2012).
- [24] R. F. da Costa, M. H. F. Bettega, M. T. do N. Varella, E. M. de Oliveira, and M. A. P. Lima, *Phys. Rev. A* **90**, 052707 (2014).
- [25] R. F. da Costa, E. M. de Oliveira, M. H. F. Bettega, M. T. do N. Varella, D. B. Jones, M. J. Brunger, F. Blanco, R. Colmenares, P. Limão-Vieira, G. García *et al.*, *J. Chem. Phys.* **142**, 104304 (2015).
- [26] R. F. da Costa, M. T. do N. Varella, M. H. F. Bettega, R. F. Neves, M. C. A. Lopes, F. Blanco, G. García, D. B. Jones, M. J. Brunger, and M. A. P. Lima, *J. Chem. Phys.* **144**, 124310 (2016).
- [27] R. F. da Costa, J. Ruivo, F. Kossoski, M. T. do N. Varella, M. H. F. Bettega, D. B. Jones, M. Brunger, and M. A. P. Lima, *J. Chem. Phys.* **149**, 174308 (2018).
- [28] A. G. Falkowski, M. A. P. Lima, and F. Kossoski, *J. Chem. Phys.* **152**, 244302 (2020).
- [29] G. M. Moreira, F. Kossoski, M. H. F. Bettega, and R. F. da Costa, *J. Phys. B: At. Mol. Opt. Phys.* **53**, 085002 (2020).
- [30] A. G. Falkowski, R. F. da Costa, F. Kossoski, M. J. Brunger, and M. A. P. Lima, *Eur. Phys. J. D* **75**, 310 (2021).
- [31] P. A. S. Randi, G. M. Moreira, and M. H. F. Bettega, *Eur. Phys. J. D* **75**, 306 (2021).
- [32] P. A. S. Randi, G. M. Moreira, and M. H. F. Bettega, *Phys. Rev. A* **107**, 012806 (2023).
- [33] A. d. A. Cadena, A. G. Falkowski, R. Pocaroba, R. Jones, M. Mathur, J. G. Childers, A. S. Barbosa, M. H. F. Bettega, R. F. da Costa, M. A. P. Lima, F. Kossoski, and M. A. Khakoo, *Phys. Rev. A* **106**, 062825 (2022).
- [34] A. G. Falkowski, R. F. da Costa, M. A. P. Lima, A. de A. Cadena, R. Pocaroba, R. Jones, M. Mathur, J. G. Childers, M. A. Khakoo, and F. Kossoski, *J. Chem. Phys.* **159**, 194301 (2023).
- [35] C. J. Joachain, *Quantum Collision Theory* (North-Holland, Amsterdam, 1975).
- [36] J. D. Gorfinkiel and J. Tennyson, *J. Phys. B: At. Mol. Opt. Phys.* **38**, 1607 (2005).
- [37] M. C. Zammit, J. S. Savage, D. V. Fursa, and I. Bray, *Phys. Rev. Lett.* **116**, 233201 (2016).
- [38] M.-T. Lee, I. Iga, L. E. Machado, L. Brescansin, E. A. y Castro, I. P. Sanches, and G. L. C. de Souza, *J. Electron Spectrosc. Relat. Phenom.* **155**, 14 (2007).
- [39] Y.-K. Kim and M. E. Rudd, *Phys. Rev. A* **50**, 3954 (1994).
- [40] L. F. Canto and M. S. Hussein, *Scattering Theory of Molecules, Atoms, and Nuclei* (World Scientific, Singapore, 2013).
- [41] A. G. Falkowski, M. H. Bettega, M. A. Lima, and L. G. Ferreira, *Eur. Phys. J. D* **75**, 308 (2021).
- [42] R. D. Johnson, NIST Computational Chemistry Comparison and Benchmark Database, NIST Standard Reference Database Number 101 Release 22, May 2022, <http://cccbdb.nist.gov/>.
- [43] A. P. P. Natalense, C. S. Sartori, L. G. Ferreira, and M. A. P. Lima, *Phys. Rev. A* **54**, 5435 (1996).
- [44] R. F. da Costa, F. J. da Paixão, and M. A. P. Lima, *J. Phys. B: At. Mol. Opt. Phys.* **38**, 815 (2005).
- [45] C. W. Bauschlicher, *J. Chem. Phys.* **72**, 880 (1980).
- [46] G. M. Barca, C. Bertoni, L. Carrington, D. Datta, N. De Silva, J. E. Deustua, D. G. Fedorov, J. R. Gour, A. O. Gunina, E. Guidez *et al.*, *J. Chem. Phys.* **152**, 154102 (2020).
- [47] T. Sharp, *At. Data Nucl. Data Tables* **2**, 119 (1970).
- [48] T. Meltzer, J. Tennyson, Z. Masin, M. C. Zammit, L. H. Scarlett, D. V. Fursa, and I. Bray, *J. Phys. B: At. Mol. Opt. Phys.* **53**, 145204 (2020).
- [49] J. Wrkich, D. Mathews, I. Kanik, S. Trajmar, and M. A. Khakoo, *J. Phys. B: At. Mol. Opt. Phys.* **35**, 4695 (2002).
- [50] L. R. Hargreaves, S. Bhari, B. Adjari, X. Liu, R. Laher, M. Zammit, J. S. Savage, D. V. Fursa, I. Bray, and M. A. Khakoo, *J. Phys. B: At. Mol. Opt. Phys.* **50**, 225203 (2017).
- [51] S. K. Srivastava, A. Chutjian, and S. Trajmar, *J. Chem. Phys.* **63**, 2659 (1975).
- [52] T. W. Shyn and W. E. Sharp, *Phys. Rev. A* **24**, 1734 (1981).
- [53] J. Muse, H. Silva, M. C. A. Lopes, and M. Khakoo, *J. Phys. B: At. Mol. Opt. Phys.* **41**, 095203 (2008).
- [54] K. R. Hoffman, M. S. Dababneh, Y.-F. Hsieh, W. E. Kauppila, V. Pol, J. H. Smart, and T. S. Stein, *Phys. Rev. A* **25**, 1393 (1982).
- [55] M. A. Khakoo and J. Segura, *J. Phys. B: At. Mol. Opt. Phys.* **27**, 2355 (1994).
- [56] M. Zawadzki, R. Wright, G. Dolmat, M. F. Martin, B. Diaz, L. Hargreaves, D. Coleman, D. V. Fursa, M. C. Zammit, L. H. Scarlett, J. K. Tapley, J. S. Savage, I. Bray, and M. A. Khakoo, *Phys. Rev. A* **98**, 062704 (2018).
- [57] Y.-C. Wang, G. Visentin, L. G. Jiao, and S. Fritzsche, *Phys. Rev. A* **109**, 022804 (2024).
- [58] S. Singh, R. Nagma, J. Kaur, and B. Antony, *J. Chem. Phys.* **145**, 034309 (2016).